Available online at www.sciencedirect.com
SCIENCE DIRECT®
Journal of Magnetic Resonance 162 (2003) 241–249
JMR Journal of Magnetic Resonance
www.elsevier.com/locate/jmr

Laser-polarized ^{129}Xe NMR at 1.88 T and 8.5 mT: a signal-to-noise ratio comparison

Albert R. Cross,* Mark McDonald, Juan Parra Robles, and Giles E. Santyr

Department of Physics, Carleton University, Herzberg Laboratories, 1125 Colonel By Drive, Ottawa, Ont., Canada K1S 5B6

Received 20 August 2002; revised 4 April 2003

Abstract

The signal-to-noise ratio of nuclear magnetic resonance signals from laser-polarized ^{129}Xe gas was investigated at 8.5 mT and compared to that of signals acquired at 1.88 T. A dedicated 8.5 mT resistive magnet was constructed and used to acquire the signals. The SNR for 1 atm of xenon gas with a polarization of 1% was measured to be 1900 at a field of 1.88 T. Under identical acquisition conditions, the SNR at 8.5 mT was about 60 (or 32 times lower). After measuring and including all of the electrical factors of the detection systems at each field strength, theory indicates the SNR value measured at 8.5 mT should be about 36 times lower. Considering the widely differing frequencies and completely different detection systems the agreement is quite good and indicates that extrapolating the frequency dependence of the SNR down to very low fields does work as long as the detection system parameters are carefully accounted for. This work suggests that magnetic resonance (MR) imaging is achievable on ideal gas samples at 8.5 mT using laser-polarized ^{129}Xe gas down to the practical resolution limit of about 0.5 mm, although the SNR will be very low ($\sim$1.4). The feasibility of imaging small animals at 8.5 mT is discussed and it is suggested that a field of about 50 mT is required.

Keywords: Laser polarized; ^{129}Xe; SNR; Low field; Spin exchange

1. Introduction

The use of laser polarization to selectively populate the nuclear Zeeman energy levels and therefore increase signal strength was first applied to magnetic resonance (MR) imaging in 1994 [1]. Population differences of the nuclear Zeeman energy levels determine the degree of polarization of the nuclei and thus the signal strength. In conventional nuclear magnetic resonance (NMR), the polarization relies on thermal energy transfer and is approximately a linear function of the magnetic field strength. The polarization of laser-polarized nuclei is not strongly dependent upon the field strength, instead relying on other independent variables such as the laser power and the gas mixture [2]. The MR signal strength resulting from a given polarization is therefore expected to have approximately a linear dependence on field strength for laser-polarized gas rather than the quadratic dependence of conventional thermally polarized samples. As a result, laser-polarized MR experiments can be performed at considerably lower magnetic field strengths ($B_0 \ll 1$ T) than clinical MR imaging, which is typically carried out at 1.5 T.

Since field strength is directly proportional to frequency, the final signal-to-noise (SNR) advantage of laser-polarized over thermally polarized experiments as the field strength is lowered depends on the frequency dependence of the noise source [3,4]. The two main noise sources in MR imaging are thermal Johnson noise originating in the conductive material of the coil and noise resulting from the coupling of the coil to the thermal noise generated by the conductive sample. These two noise sources are usually referred to as coil noise and sample noise. The frequency dependence of the coil performance as well as other electronic factors will determine the overall SNR observed.

Laser-polarized noble gases provide exciting possibilities for performing MR imaging at low fields ($<$0.1 T). The benefits of low-field MR imaging are potentially numerous [5]. A low-field magnet would not require superconducting technology to maintain its field

* Corresponding author. Fax: +613-520-4061.
E-mail address: across@physics.carleton.ca (A.R. Cross).

1090-7807/03/$ - see front matter © 2003 Elsevier Science (USA). All rights reserved.
doi:10.1016/S1090-7807(03)00121-6

strength and could instead rely upon more conventional resistive or permanent magnet technology which could be less expensive and more portable. Also, the low-field strength results in a reduced operating, or Larmor, frequency (kHz instead of MHz) which simplifies the RF electronics. These lower frequencies also have large skin depths, allowing gas space imaging inside conductive materials [6]. Finally, at low-magnetic fields there is a reduced effect of magnetic susceptibility heterogeneity and chemical shift, resulting in a longer T_2^* and improved spectral bandwidth and reduced distortion.

Since the introduction of laser-polarized noble gases to MR imaging, there have been several investigations of their uses at low field. Darrasse et al. demonstrated laser-polarized ^{3}He human lung imaging at 0.1 T [7], while Saam and coworkers obtained one-dimensional profiles of cells filled with laser-polarized ^{3}He at 3.1 mT [8]. In addition, using superconductive quantum interference devices (SQUIDS), Augustine et al. imaged laser-polarized ^{3}He and solid ^{129}Xe at liquid helium temperatures (4 K) and 54 μT [9]. Most recently, Wong et al. demonstrated fast, single-scan 2D imaging at 2.1 mT of laser-polarized ^{3}He in sealed glass phantoms [6] and excised rat lungs [5]. Finally, Yang et al. obtained a low-field laser-polarized ^{129}Xe image of a live rat lung [10] by lowering the field strength of a superconducting magnet from 1.5 T to 15.0 mT.

The purpose of this work was to compare the SNR at 1.88 T and 8.5 mT as a step towards the imaging of laser-polarized ^{129}Xe at 8.5 mT. The design and construction of a prototype NMR system for laser-polarized ^{129}Xe are described as well as the experimental methodology for acquiring laser-polarized ^{129}Xe gas signals. Using both laser-polarized and thermally polarized SNR measurements, a theoretical and experimentally validated comparison of the SNR of the low-field system with the SNR of a 1.88 T superconducting system is presented. The availability of enough SNR to image small animals at the practical resolution limit is also discussed.

2. Materials and methods

2.1. Low-field NMR system

A block diagram of the complete 8.5 mT apparatus is shown in Fig. 1. This diagram shows the three main sections of the apparatus: the resistive electromagnet (medium gray), the laser polarization hardware (dark gray), and the NMR spectrometer (light gray).

The electromagnet was designed based on a modification [11] of Garrett's theory of axial symmetric magnetic fields [12]. This theory describes the positioning of pairs of current loop distributions such that the dominant non-symmetric terms in the field expansions of an individual loop cancel in the region between the loops producing a homogeneous field. The design criteria were to produce a 8.5 mT field (which corresponds to a Larmor frequency of 100 kHz for ^{129}Xe) with an inhomogeneity of less than 1% over a 10 cm diameter spherical volume (DSV) using a 80 V, 10 A power supply. Since the resistance from the total length of wire becomes a barrier in attempting to add more loops, a simple two-loop or split-solenoid design was found to best meet these criteria. A longitudinal cross-sectional view of the magnet indicating the coil-winding geometry is shown in Fig. 2. The electromagnet coil

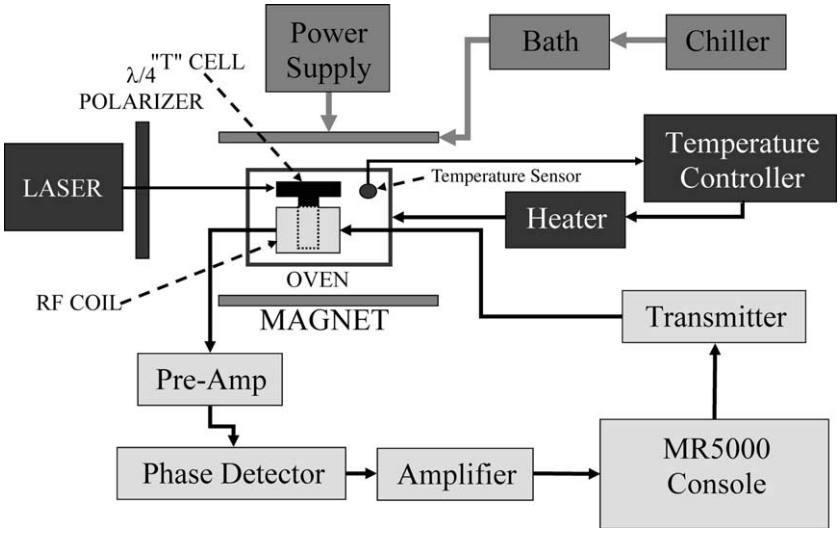

Fig. 1. A block diagram of the experimental setup used. The grayscale is used to indicate the three main sections of the apparatus: the resistive electromagnet (medium gray), the laser polarization (dark gray), and the NMR spectrometer (light gray). A sample cell (black) is laser-polarized inside the magnet and kept at a constant temperature (88 °C) using an oven and temperature controller.

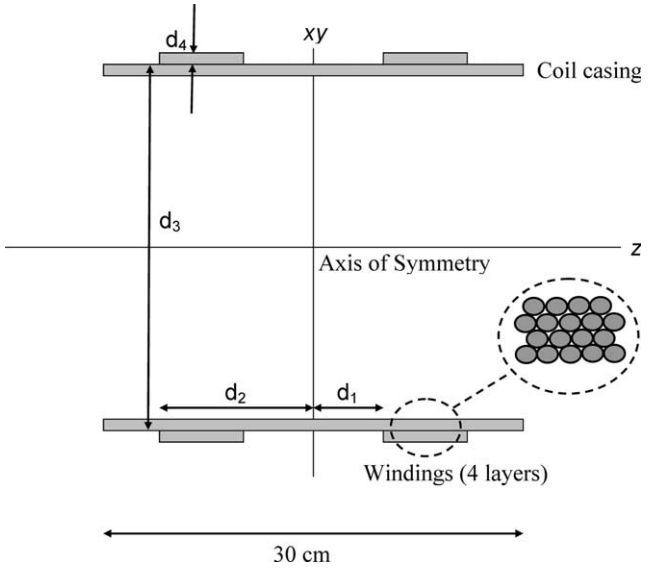

Fig. 2. A longitudinal cross-sectional view of the low-field resistive electromagnet. The split-solenoid design is characterized by two bands of windings, each 6 cm wide and four layers of wire deep. The bands are spaced 10 cm apart. Specifications are provided in Table 1. The inset shows the winding configuration of the coil.

Table 1
Mechanical and electrical specifications of the resistive electromagnet

Mechanical characteristics	
d_1	5.00 ± 0.05 cm
d_2	11.00 ± 0.05 cm
d_3	13.56 ± 0.05 cm
d_4	0.60 ± 0.05 cm
N	8.29 turns/cm
No. layers	4
Tot. turns	428 ± 4
Wire gauge (AWG)	18
Electrical characteristics	
R	$9.1 \pm 0.1\ \Omega$
B_z	12.34 G/A
I	6.880 ± 0.001 A
P	430 ± 5 W

The physical dimensions correspond to those in Fig. 2.

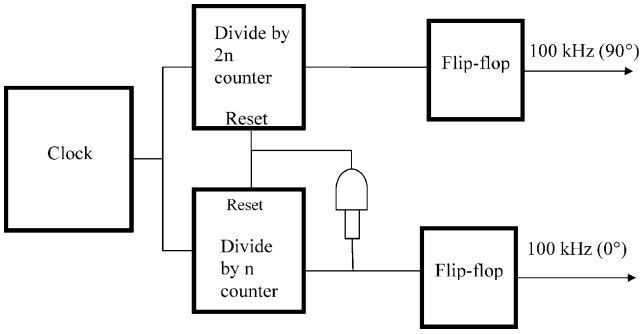

Fig. 3. Modified reference signal circuit. The divide by $2n$ counter is reset on the output of the divide by n counter. The result is a signal with the same frequency delayed by exactly half of the counter cycle or 1/4 of a period.

was wound using 18 AWG wire on a fiberglass-reinforced cardboard former which was 30 cm in inner diameter. Epoxy resin was used to fix the wires in position. Two DC power supplies (Sorensen SRL 40–50 and Harrison Laboratories Model 814A) were cascaded in series to provide the necessary voltage. The magnet was cooled using chilled antifreeze circulated through 3/16 in. copper tubing wound on the outside of the windings. The magnetic field of the coil was mapped using a FW Bell 640 Gaussmeter (Orlando, FL, USA) with an axial magnitude probe. Current fluctuations were on the order of ± 1.0 mA, or equivalently $\pm 0.1\ \mu$T or ± 15 Hz in the signal frequency. The physical and electrical operating characteristics of the magnet are summarized in Table 1.

The 8.5 mT NMR spectrometer was based on the polarimeter design of Saam and Conradi [8]. This design was modified to include quadrature phase detection and an interface to the console described below (Section 2.2) consisting of an inverting buffer between the transmitter blanking output (which is TTL) of the console and the 100 kHz transmitter. Appropriate modifications to the output circuitry of the 100 kHz phase detection to allow for DC offset adjustment and to modify the impedance of the phase detector output to be compatible with the expected 50 Ω input of the console digitizer inputs. A block diagram of the quadrature detection modifications is provided in Fig. 3. The RF coil used was a Helmholtz design tuned to 100 kHz with an inside diameter of 1 cm and a length of 1.58 cm. The windings on each side of the Helmholtz pair are extended over a distance of 0.485 cm with the gap between the pair being 0.610 cm. The thickness of the region occupying the windings is 0.195 cm resulting in a total outside diameter of each winding being 1.590 cm. The total number of turns of the coil was 560 of 34 AWG coated copper magnet wire. The coil was encased in an aluminum box 3 mm thick to shield the coil from any extraneous electromagnetic interference (e.g., computer monitors, power supplies, etc.). A 2.5 cm ID hole was cut in the box to allow the laser beam to reach the sample. The hole did not decrease the effectiveness of the shield.

2.2. High-field NMR system

The 1.88 T spectrometer consisted of a MRRS (formerly SMIS, Surrey Medical Imaging Systems, Surrey, UK) MR5000 console interfaced to a 30 cm bore superconducting magnet (Magnex Scientific, Concord CA, USA). The receiver coil was a 14 turn solenoid coil (1 cm inner diameter, 5.4 cm length, 12 AWG wire) tuned to the ^{129}Xe resonant frequency (22.172 MHz) and matched to a 50 Ω impedance.

2.3. Laser polarization

A 30 W Al–Ga–As diode array laser emitting at 794.8 nm (Opto-Power, Tucson, AZ) was used to polarize the sample. All samples were polarized at a field strength of about 8.5 mT. For the low-field case, polarization was done inside the 8.5 mT magnet itself while for the 1.88 T case it was done in the fringe field of the 1.88 T superconducting magnet and then transferred to the detection field. In both cases, the beam was circularly polarized using a $\lambda/4$ filter (Opto-Power, Tucson, AZ) and directed parallel to the magnetic field. The laser-polarized sample contained 730 mbar natural abundance xenon gas, 102 mbar N_2 and a few milligrams of Rb metal. For all cases, natural abundance xenon gas was used (26% ^{129}Xe), hereafter referred to as xenon gas. The glass walls of the sample cell were coated with SurfaSil (Pierce Chemical Laboratories) to reduce the relaxation of the xenon gas due to wall collisions. The sample geometry was in the shape of a "T" (see Fig. 1) and will hereafter be referred to as the T sample. The tail of the T sample had an outside diameter of 1.0 cm and extended 8 cm from the side of a 4 cm long cylindrical piece which had an outside diameter of 3.7 cm. This geometry allowed the sample to be polarized with the laser (beam diameter about 2.5 cm) while residing in the coil. During polarization, the sample was maintained at 88 °C in order to maintain the rubidium as a vapor. The polarization time was approximately 20 min. The optimization of both temperature and polarization time are described in more detail elsewhere [13].

The polarization was calculated from the ratio (S_{LP}/S_{TH}) of laser-polarized signal, S_{LP}, and thermal signal S_{TH} according to:

$$P_{LP} = \left(\frac{S_{LP}}{S_{TH}}\right)\frac{N_{TH}P_{TH}}{N_{LP}}, \tag{1}$$

where P is the polarization and N is the density of xenon atoms. The subscripts TH and LP indicate thermally polarized and laser-polarized variables, respectively. The density terms were replaced by the appropriate pressure terms (since the volume was the same). The thermal polarization (P_{TH}) was calculated to be 1.8033×10^{-6} from the theoretical Boltzmann distribution for the field strength of 1.8839 T and assuming a temperature of 293 K. For the acquisition of thermally polarized xenon signals, a separate calibration sample was used. The diameter of the calibration sample was 1.0 cm with a length of 13.5 cm. The sample was filled with 5140 mbar STP of xenon gas and about 3800 mbar STP of oxygen gas. The presence of oxygen in the calibration sample lowers the T_1 relaxation time of the xenon to about 510 ms at 1.88 T, thereby reducing the repetition time needed to acquire the full signal with a 90° pulse. Furthermore, the elevated xenon pressure increased the low-thermal signal amplitude.

2.4. SNR measurements

NMR signals were obtained by acquiring a free induction decay (FID) at each field strength. Signal amplitudes were estimated by fitting an exponentially decaying sine function to the real and imaginary FID signals. The amplitude was then calculated as the root mean square of the two values extrapolated to zero time. The noise was estimated as the standard deviation of the signal from an empty coil. SNR measurements at 1.88 T were acquired using a 90° pulse with a dwell time of 100 μs. The RF pulse tip angle was calibrated using fast ($T_R \ll T_1$) repetition of a low-flip angle (α) pulse on a laser-polarized sample [14]. The ratio of the signal amplitude following successive pulses is $\cos(\alpha)$. This procedure was repeated for a variety of tip angles to determine that a 90° pulse corresponded to a pulse length of 54 μs. The laser-polarized signals were measured from a single acquisition using the T sample previously described while the thermally polarized signal used the high-pressure calibration sample (5140 mbar xenon) with 128 signal averages. The repetition time during the thermal signal acquisition was 4 s which is approximately 8 times T_1 and therefore long enough to give full recovery of the signal.

A concern in the comparison of theory and experiment was the possible confounding effect of radiation damping and its possible effect on the tip angle calibration. Radiation damping is known to occur whenever polarization is very large and was a prominent factor in a similar work involving laser-polarized ^{3}He [5]. Radiation damping was investigated in this study using three different techniques. The first was to look for abnormalities in the FID using a flip angle $\alpha > 180°$, the second was to plot the signal intensity against flip angle ($0° < \alpha < 120°$) and the third to compare the tip angle calibration for different acquisition times along the FIDs. In all three cases radiation damping was not found to be present and was deemed not to be an issue for these experiments.

Even with the aid of the high-pressure (5140 mbar) sample cell, detection of a thermally polarized xenon signal at 8.5 mT was beyond the capability of the 8.5 mT system. Therefore, the thermal xenon signal strength at 8.5 mT was estimated using the proton signal of a water sample by lowering the field strength of the electromagnet to 2.3 mT to give the same Larmor frequency ($f_0 = 100$ kHz) and correcting according to:

$$S_{Xe} = S_H\frac{\gamma_{Xe}N_{Xe}}{\gamma_H N_H}, \tag{2}$$

where $N_{Xe} = 4.6591 \times 10^{24}$ atoms/m^3 and $N_H = 6.6918 \times 10^{28}$ atoms/m^3 and equal sample volumes have been assumed. N_{Xe} is the number of ^{129}Xe nuclei and was calculated from the known pressure (730 mbar) according to the ideal gas law. N_H was calculated based on the

molecular weight (18 g/mol) and density (1 g/cm^3) of water. Thermal proton signals were acquired with a dwell time of 20 μs and a 90° pulse width of 114 μs. One thousand (1000) signal averages were used with a repetition time of 2.5 s. The water sample (diameter 1.0 cm OD, length 7.2 cm) contained 0.56 mM of Gd-DTPA (Prohance, Squibb Diagnostics, Montreal) to speed up the acquisition and prevent saturation. At 1.88 T the T_1 of the water sample was 365 ms. Although the T_1 was not explicitly measured at 8.5 mT, negligible change in signal intensity with a repetition time of 1.5 s was observed. Laser-polarized signals at 8.5 mT were obtained from a single acquisition using the T sample cell previously described. A dwell time of 20 μs and a 90° pulse width of 411 μs were used. The RF pulse tip angle for the 8.5 mT system was calibrated on the laser-polarized xenon sample in the manner previously described for the 1.88 T RF pulse tip angle calibration. The 90° pulse length for the proton case was calculated from that found for xenon but taking into account the gyromagnetic ratio difference.

2.5. SNR calculations

For an ideal solenoid coil, the SNR can be represented as [15]:

$$\mathrm{SNR} = K\eta M_0\sqrt{\frac{\mu_0 Q\omega_0 V_c}{4FkT\Delta f}}, \tag{3}$$

where K is a numerical factor representing the RF field inhomogeneity (~1), η is the filling factor, M_0 is the magnetization, μ_0 is the permeability of free space, Q is the quality factor of the RF coil, $\omega_0 = 2\pi f_0$, where f_0 is the resonance frequency, V_c is the volume of the coil, F is the noise figure of the receiver, k is the Boltzmann constant, T is the coil temperature, and Δf is the bandwidth of the receiver.

To calculate a theoretical estimate of the expected SNR, these factors were first estimated independently as follows. The Q values of the RF coils were determined by measuring the bandwidth, Δf_c, of each coil and dividing into the resonance frequency, f_0:

$$Q = \frac{f_0}{\Delta f_c}. \tag{4}$$

In the case of the 8.5 mT coil, the Q was measured both air-filled and water-filled. This was to check for differences in the loading of the coil when acquiring the proton signal for the 8.5 mT polarization measurement. At 100 kHz, the Q was unaffected by the loading of the doped-water sample.

The noise figures of the two receivers were measured with a liquid nitrogen test [16] using:

$$F = 10\log\left(1 - \frac{77}{T}\right) - 10\log\left(1 - \frac{1}{\alpha^2}\right), \tag{5}$$

where T is the room temperature in Kelvin (K) and α is the signal attenuation factor. The noise was estimated as the standard deviation of the recorded signals. The error in the noise figure was estimated from the standard deviation of 10 consecutive measurements of the noise. For the 1.88 T measurements, a 50 Ω resistor was used while for the 8.5 mT measurements, a 2000 Ω resistor was used. This was due to the differences in input impedance of the two receivers.

The coil radius (r_c in Table 3) of each coil was recorded as the mean of the inner and outer radii of the coil. The coil temperatures were taken to be room temperature (298 K) in all cases except for the 8.5 mT laser-polarized signals, where $T = 361$ K (88 °C), the temperature of the oven in which the sample cell was polarized. The receiver bandwidth, Δf, was taken to be either the sampling rate or the coil bandwidth, whichever was smaller.

The combined contribution from the factors $K\eta$ were accounted for by first numerically calculating the field distribution produced by the two coils using the static Biot–Savart Law and the current distribution produced by the coil windings. Fig. 4 displays the field intensity resulting from this calculation normalized to the field intensity at the center of the coil. The factor $K\eta$ was then determined by numerically integrating the normalized field and dividing by the coil volume. The simulated field was integrated over the length of the tail of the T sample (8 cm). Since the sample extends far outside the coil, Fig. 4 shows that the field was dropped to less than 10% of the central field in all cases. Since this is a transmit and a receive coil, an extra $\sin(\frac{\pi}{2}\frac{B_1(r,z)}{B_1(0,0)})$ factor has been added to account for the excitation distribution and the sensitivity on reception. With these conditions accounted

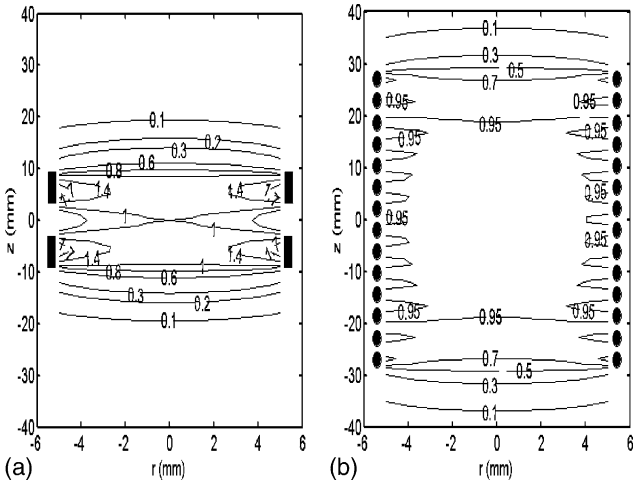

Fig. 4. A cross-sectional diagram of the normalized field distribution for (a) the 8.5 mT Helmholtz coil and (b) the 1.88 T solenoid coil. The field has been normalized to the field in the central region of the coils. The solid rectangles and ovals indicate the positions of the wire windings. The end of the contour lines indicate the edges of the sample.

for, the combined $K\eta$ factors were determined to be 0.994 and 1.31 for the solenoid and Helmholtz coil, respectively.

3. Results

Fig. 5 displays a sample FID of each of the four cases measured (8.5 mT and 1.88 T; laser-polarized and thermal). The 8.5 mT water (proton) signal (Fig. 5a) was acquired with 1000 signal averages while the 1.88 T thermal xenon signal (Fig. 5c) was acquired with 128 signal averages. Figs. 5b and d are laser-polarized xenon signals at 8.5 mT and 1.88 T, respectively. The laser-polarized xenon signals were acquired with a single scan. The y-axis in all cases is arbitrary and absolute signal strengths in this figure are not directly comparable since different densities (water, gas pressures), polarization levels and amplifications exist in the four different cases. A summary of the SNR values extracted for these four experimental cases is presented in Table 2. To correct for the difference in densities between experiments, the values in Table 2 have been normalized to the SNR achieved for 1 atm of xenon gas. In the case of laser-polarized samples, the SNR values have also been normalized to a polarization level of 1%.

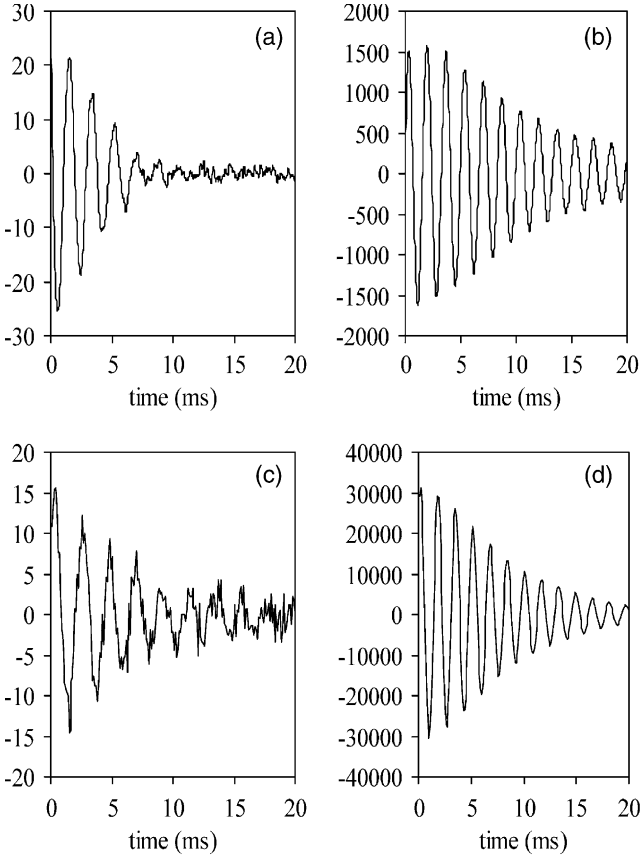

Fig. 5. A comparison of typical thermally and laser-polarized signals at 1.88 T and 8.5 mT. (a) Thermally polarized ^{1}H (water) at 2.3 mT, 1000 signal averages. (b) Laser-polarized xenon gas at 8.5 mT. (c) Thermally polarized xenon gas at 1.88 T, 128 signal averages. (d) Laser-polarized xenon gas at 1.88 T. All intensities are in arbitrary units without any corrections. The laser-polarized signals (b,d) were acquired with a single scan.

Table 2
SNR measurements

B_0	1.88 T	8.5 mT
SNR_{TH}	$(3.44 \pm 0.28) \times 10^{-1}$	$(4.78 \pm 0.25) \times 10^{-5}$
SNR_{LP}	$(1.90 \pm 0.21) \times 10^{3}$	58.8 ± 1.0

The values have been scaled to 1 atm xenon and for, the laser-polarized cases, the values have been normalized to a polarization level of 1%.

Table 3
Parameters used to estimate the ratio of SNR using two different spectrometers at two different static field strengths

B_0	1.88 T	8.5 mT
$K\eta$[a]	0.994	1.31
r_c (cm)	0.7363 ± 0.0087	0.7025 ± 0.0087
P_{LP}	0.0316 ± 0.002	0.0231 ± 0.002
P_{TH}	1.8033×10^{-6}	8.1322×10^{-9}
Q	198 ± 11	29.4 ± 3.1
V_c (cm^3)	4.24 ± 0.09	1.30 ± 0.02
F (dB)	4.26 ± 0.11	4.2 ± 0.6
T_{LP} (K)	293 ± 1	361 ± 1
T_{TH} (K)	293 ± 1	298 ± 1
Δf_{LP} (Hz)	10,000	3400 ± 355
Δf_{TH} (Hz)	10,000	3400 ± 355

The thermal polarizations (P_{TH}) are calculated values, all the others are measured.
[a] From the numerical simulation.

Table 4
Comparison of the measured ratios of SNR

Polarization	Thermal ($\times 10^3$)	Laser
R_M	7.17 ± 0.95	32.2 ± 4.1
R_T	7.32 ± 0.19	36.3 ± 6.0
R_M/R_T	0.98 ± 0.29	0.89 ± 0.26

$R_M = (SNR_{HF}/SNR_{LF})$ for measured values. $R_T = (SNR_{HF}/SNR_{LF})$ for theoretical values.

The list of electronic parameters and their values used in the theoretical calculations of SNR are given in Table 3. The laser polarization factors (P_{LP}) and the calculated thermal polarization factors (P_{TH}) for both 1.88 T and 8.5 mT are presented. The noise figure, F, was determined for both systems, using Eq. (5).

Table 4 presents the results of the theoretical calculation of the SNR enhancement ratio (R_T = [theoretical high-field SNR]/ [theoretical low-field SNR]) for the laser-polarized and thermally polarized cases, respectively. The corresponding ratio (R_M = [measured high-field SNR]/ [measured low-field SNR]) computed from the SNR measurements in Table 2 are also presented in Table 4.

4. Discussion

The purpose of this work was to measure the SNR of laser-polarized xenon at 1.88 T and at 8.5 mT and compare the experimental values with theoretical expectations (Eq. (3)). A commercially available MR system was used for the 1.88 T measurements, while both a magnet and a detection system were built for the 8.5 mT measurements. Fig. 5 displays signals which were detected by both systems. The two laser-polarized signals (Figs. 5b and d) demonstrate high SNR at both field strengths. This is a demonstration of the performance of the constructed apparatus for detecting laser-polarized xenon gas NMR signals at 8.5 mT. The adequate homogeneity of the 8.5-mT magnet is indicated by a visual comparison of Figs. 5b and d, revealing that the rate of decay of the signals is comparable. The successful acquisition of the 2.3-mT water signal (Fig. 5a) demonstrates that the temporal stability of the 100 kHz system is adequate to perform signal averaging. As already stated, the temporal fluctuations of the magnet power supply were measured to be about 0.015%.

A comparison of the SNR at 1.88 T and 8.5 mT can be made by taking the ratio of SNRs at these two field strengths directly. Using Eq. (3), the ratio is:

$$\frac{\mathrm{SNR_{HF}}}{\mathrm{SNR_{LF}}} = \frac{(K\eta P)_{\mathrm{HF}}}{(K\eta P)_{\mathrm{LF}}}\sqrt{\frac{(Qf_0V_c/FT\Delta f)_{\mathrm{HF}}}{(Qf_0V_c/FT\Delta f)_{\mathrm{LF}}}}, \tag{6}$$

where P is the polarization factor and the HF and LF subscripts represent the high and low-field strengths of 1.88 T and 8.5 mT, respectively. Using this expression, the ratio of SNRs was calculated and compared to the measured quantities for both the laser-polarized and thermally polarized experiments. Using Eq. (6) with all of the measured electronic and acquisition parameters, the theoretical result (R_T) was 36.3 ± 6.0 for the laser-polarized case and 7320 ± 1200 for the thermal case. The ratio derived from the measured SNR at each field (R_M) was 32.2 ± 4.1 for the laser-polarized case and 7170 ± 950 for the thermal case.

The data in Tables 2 and 4 give good correspondence between theory and experiment using Eq. (6). In these theoretical calculations, the measured quality factor Q of each coil has been inserted. Therefore the field dependence of the Q of the coil is necessary in determining the field or equivalently the frequency dependence of the SNR. Hoult and Richards [3] have measured the quality factors of equivalent coils at different frequencies and found an approximate square root dependence with frequency with coil dominated noise. This would give an expected SNR frequency dependence of $f^{3/4}$ for laser-polarized signals and the well-known conclusion of $f^{7/4}$ for thermally polarized signals.

Neglecting the frequency dependence of the coil leads to the conclusion that the laser-polarized SNR will be proportional to B_0 [5]. It should be noted the equations in this manuscript and reference [5] are equivalent for a solenoid [3] except that the frequency dependence of the coil and noise have been re-distributed in the terms of the equations. Eq. (3) indicates that if the same Q could be achieved at each field, a square root dependence of the SNR on frequency is possible, however, it is unlikely that the same quality factor can be achieved at 8.5 mT as at 1.88 T if both systems are performing optimally. Fig. 6 shows the data points and these possible theoretical trends (scaled by the measured SNR at 1.88 T). This figure demonstrates that the observed SNR at 8.5 mT is best estimated by the trend that includes the frequency-dependent coil factors. This also demonstrates that neglecting the frequency dependence of the coil terms in these two formulations of the SNR leads to different conclusions of the dependence of the SNR on frequency.

With the data, the prospects for imaging can be estimated. In considering the application of laser-polarized xenon gas to image the lungs of a living animal (e.g., rat) the resolution limit due to field homogeneity and gas diffusion need to be estimated. Following the treatment of Callaghan [17], with a T_2^* of 100 ms and a diffusion coefficient for xenon of 1.13×10^{-5} m^2/s the optimum acquisition time would be 31.8 ms and the maximum allowable gradient would be 16.6 mT/m. From these values, the T_2^* resolution limit (Δx_{opt}) would be 0.1 mm and a corresponding diffusion resolution factor (Δx_{diff}) of 0.85 mm for a resolution limit of 0.27 mm. Although the maximum resolution is 0.27 mm in practice the 8.5-mT system is limited in bandwidth by

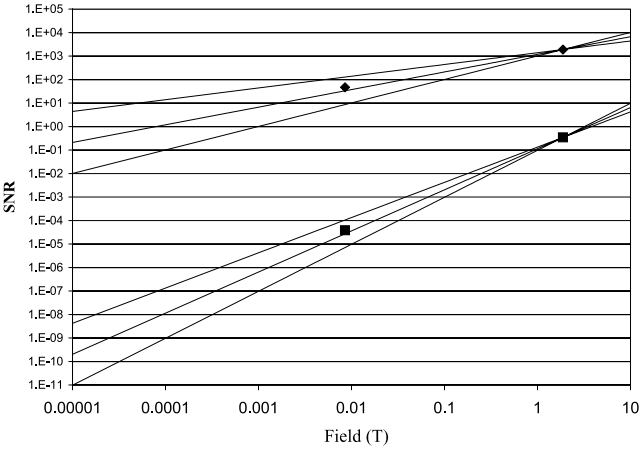

Fig. 6. A plot of the possible SNR dependence on the magnetic field. The square points are the measured thermally polarized SNR values and the diamonds are the laser-polarized SNR values. The 8.5-mT values have been corrected for the acquisition bandwidths, and the coil volumes (Table 3). The solid lines represent the theoretical trends normalized to the 1.88-T SNR value. For the laser-polarized curves (upper set) the upper, middle, and lower lines have a field dependence (B) of $B_{1/2}$, $B_{3/4}$, and B_1, respectively. For the thermally polarized curves (lower set) the upper, middle, and lower lines have a field dependence (B) of $B_{3/2}$, $B_{7/4}$, and B_2, respectively.

the Q of the coil and thus for a 32×32 image acquired with a sweep width of 3 kHz and the diffusion limited maximum gradient of 16.6 mT/m a practical resolution limit is about 0.5 mm.

At these low frequencies, coil noise should dominate over sample noise [4,5] and therefore the SNR measured on these ideal gas samples can be used to estimate if there is enough SNR to image at the maximum practical resolution even in the presence of a lossy sample like a rat. The signal-to-noise per voxel in an image (SNR_I) can be related to the signal-to-noise in the FID (SNR_F) by [17]:

$$SNR_I = \frac{4}{\pi}\frac{N}{N_O^2}(SNR_F)e^{-T_E/T_2^*}\sin(\alpha), \quad (7)$$

where N is the number of points in an $N \times N$ image and N_O are the number of pixels which lie on the object, the exponential term reflects the decay of the signal with T_2^* during the echo time T_E and $\sin(\alpha)$ accounts for the non-recoverable nature of the laser polarized magnitude. At 8.5 mT assuming a 25° pulse is used to acquire a 32×32 image, with 0.5 mm pixels (20 pixels on the 1 cm sample) and $T_E \ll T_2^*$, 1 atm of xenon polarized to 2% would be needed to give an image SNR of 5. This is encouraging, however, the realistic implementation of imaging applied to small animals would require the construction of a larger RF coil. A saddle or a birdcage coil design would be needed to accommodate a large object with axial geometry. The implementation of a birdcage coil at 100 kHz may not be feasible. In the case of a saddle coil, the electrical efficiency would reduce the SNR by a factor of 2.6–3 [3,17]. In addition, the filling factor of the lungs of a rat inside the coil will be considerably lower than that of the glass cells used in this study. If the lung volume is only half of the coil volume, the combination of saddle coil efficiency and filling factor would reduce the SNR per pixel by approximately a factor of 6. Furthermore, an animal does not expel all of the gas from its lung on each breath and at best 50% of the lung gas would be xenon. With these considerations, 7% polarization would give an image signal barely above the noise (SNR $\sim$ 1.4). For these reasons, either isotopically enriched xenon or higher field strength or both would be necessary to allow imaging of the rat lung. A factor of 4 improvement in SNR could be achieved by using isotopically enriched xenon. To avoid the expense of enriched xenon, raising the field by a factor of 5.5 ($B_0 = 47$ mT) would be needed to increase the SNR to around 5.

One fundamental difference between the 1.88-T and the 8.5-mT parameters is that in the 1.88-T case the bandwidth is determined by the digitizer while in the 8.5-mT case it is determined by the coil. Improvements to the system through increases in Q will further improve the SNR by decreasing the bandwidth. However, at 3400 Hz, the bandwidth is already getting narrow for imaging and thus improvements to the coil are not a practical strategy to further improve the SNR for imaging at these frequencies. This is a problem inherent to very low frequency imaging systems. At best, a factor of 3 improvement in the SNR is achievable through electronic improvements and reducing coil temperature. The greatest possibility for SNR improvement lies in signal enhancement. In the current work, 2–3% polarization was achieved. Xenon polarization of 10–20% have been reported [18] which would provide an improvement factor of 5–7.

In this discussion, a 90° pulse has been assumed. It should be noted that as is seen in Fig. 4, the sample experiences a distribution of tip angles and in reality it is an "effective" 90° pulse. The B_1 field simulations and integration over the sample account for this distribution of tip angles. It should also be noted that the above SNR estimates are derived from the raw unfiltered SNR measured values. Optimal filtering will improve the images significantly. As well, it should be pointed out that the estimates above are for a single shot low-flip angle Fourier acquisition pulse sequence with 0.5 mm pixels. Coarser resolution will give better SNR. Projection reconstruction will also give marginally better SNR [17]. The laser-polarized signal is non-renewable and imaging is usually done as a single shot. However, multiple administrations of laser-polarized gas has been done [19]. Such strategies permit 90° tip angles and signal averaging which would greatly improve the signal to noise. EPI is also a possible strategy to more fully utilize the non-recoverable magnetization.

5. Conclusion

The SNR correspondence between the measurements and the theory is very good. The field dependence of the SNR for laser-polarized samples has been experimentally demonstrated to be consistent with a 3/4 power down to these low-magnetic field strengths. This is in agreement with conventional SNR theory for coil dominated noise and thus through this field dependence, the relative performance of a low-field system can be assessed. Caution should be used when estimating SNR since electronic factors are not field independent. The coil Q at 8.5 mT and the xenon diffusion coefficient limit the practical spatial resolution limit to about 0.5 mm. Coarse resolution imaging of ideal samples is possible at 8.5 mT with moderately polarized xenon. The practical imaging of small animals with natural abundance xenon and polarizations of 5% requires that the field be raised to about 50 mT.

Acknowledgments

The authors would like to thank Rory Schnieder of Magnex Scientific Ltd. for aid in the design of the 8.5-

mT electromagnet, Pascale Sevigny for her optimization of the xenon polarization, Jidong Xu for the initial construction of the 8.5 mT polarimeter and Steve Lang and Igor Moudrakovski at the National Research Council of Canada for constructing the T and calibration cell. This research was supported by Natural Sciences and Engineering Research Council of Canada and the Ontario Center of Excellence for Breast Cancer Imaging Research.

References

[1] M.S. Albert, G.D. Cates, B. Driehuys, W. Happer, B. Saam, C.S. Springer Jr., A. Wishnia, Biological magnetic resonance imaging using laser-polarized ^{129}Xe, Nature 370 (1994) 199–201.

[2] W. Happer, E. Miron, D. Schaefer, W.A. Van Wijngaarden, X. Zeng, Polarization of the nuclear spins of noble-gas atoms by spin exchange with optically pumped alkali-metal atoms, Phys. Rev. A 29 (1984) 3092–3110.

[3] D.I. Hoult, R.E. Richards, The signal-to-noise ratio of the nuclear magnetic resonance experiment, J. Magn. Res. 24 (1976) 71–85.

[4] D.I. Hoult, P.C. Lauterbur, The sensitivity of the zeumatographic experiment involving human samples, J. Magn. Res. 34 (1979) 425–433.

[5] G.P. Wong, C.H. Tseng, V.R. Pomeroy, R.W. Mair, D.P. Hinton, D. Hoffmann, R.E. Stoner, F.W. Hersman, D.G. Cory, R.L. Walsworth, A system for low field imaging of laser-polarized noble gas, J. Magn. Reson. 141 (1999) 217–227.

[6] C.H. Tseng, G.P. Wong, V.R. Pomeroy, R.W. Mair, D.P. Hinton, D. Hoffmann, R.E. Stoner, F.W. Hersman, D.G. Cory, R.L. Walsworth, Low-field MRI of laser polarized noble gas, Phys. Rev. Lett. 81 (1998) 3785–3788.

[7] L. Darrasse, G. Guillot, P.J. Nacher, G. Tastevin, Low field single shot ^{3}He MRI in human lungs. Proc. ISMRM. 6th Meeting, 1998, p. 449.

[8] B.T. Saam, M.S. Conradi, Low frequency NMR polarimeter for hyperpolarized gases, J. Magn. Reson. 134 (1998) 67–71.

[9] M.P. Augustine, A. Wong-Foy, J.L. Yarger, M. Tomaselli, A. Pines, D.M. Tom That, J. Clarke, Low field magnetic resonance images of polarized noble gases obtained with a DC superconducting quantum interference device, Appl. Phys. Lett. 72 (1998) 1908–1910.

[10] Y.J. Yang, M.S. Albert, K.H. Min, A.X. Zhang, G.R. Venkatesh, G.R. Gomez, D. Balamore, R.S. Hashoian, C.-L. Chin, C.H. Oh, RF coil optimization for 0.015 tesla very low-field hyperpolarized noble gas MRIs, Proc. ISMRM, 8th annual meeting, 2000, p. 1425.

[11] R.J. Hanson, F.M. Pipkin, Magnetically shielded solenoid with field of high homogeneity, Rev. Sci. Instr. 36 (1964) 179–188.

[12] M.W. Garrett, J. Appl. Phys. 22 (1951) 1091.

[13] P. Sevigny, Magnetic resonance imaging of hyperpolarized ^{129}Xe: a feasibility study for biomedical applications, M.Sc. thesis, Carleton University, 1999.

[14] B.R. Patyal, J.H. Gao, R.F. Williams, et al., Longitudinal relaxation and diffusion measurements using magnetic resonance signals from laser-hyperpolarized Xe-129 nuclei, J. Magn. Reson. 126 (1997) 58–65.

[15] H.D.W. Hill, R.E. Richards, Limits of measurement in magnetic resonance, J. Phys. E, Ser. 2 1 (1968) 977–983.

[16] C.N. Chen, D.I. Hoult, Biomedical Magnetic Resonance Technology, Adam Hilger, Bristol and New York, 1989.

[17] P.T. Callaghan, Principles of Nuclear Magnetic Resonance Microscopy, Oxford University Press, New York, 1991.

[18] J. Wolber et al., In vivo hyperpolarized Xe-129 NMR spectroscopy in tumors, Magn. Reson. Med. 46 (2001) 586–591.

[19] L.W. Hedlund, H.E. Moller, X.J. Chen, M.S. Chawla, G.P. Cofer, G.A. Johnson, Mixing oxygen with hyperpolarized ^{3}He for small-animal lung studies, NMR Biomed. 13 (2000) 202–206.